# Improving through-thickness conductivity of carbon fiber reinforced polymer using carbon nanotube/polyethylenimine at the interlaminar region

Received: 27 March 2020 | Revised: 3 June 2020 | Accepted: 3 June 2020

DOI: 10.1002/app.49749

ARTICLE

Applied Polymer SCIENCE WILEY

# Improving through-thickness conductivity of carbon fiber reinforced polymer using carbon nanotube/polyethylenimine at the interlaminar region

**Colin Robert**[1] | **Witiwat Best Thitasiri**[1] | **Dimitrios Mamalis**[1] | **Zakareya Elmo Hussein**[2] | **Muhammad Waqas**[1] | **Dipa Ray**[1] | **Norbert Radacsi**[1] | **Vasileios Koutsos**[1]

[1]School of Engineering, Institute for Materials and Processes, The University of Edinburgh, Sanderson Building, King's Buildings, Edinburgh, UK

[2]School of Engineering, Scottish Microelectronics Centre, The University of Edinburgh, Edinburgh, UK

**Correspondence**
Colin Robert, School of Engineering, Institute for Materials and Processes, The University of Edinburgh, Sanderson Building, King's Buildings, Edinburgh, EH9 3FB, UK.
Email: colin.robert@ed.ac.uk

**Funding information**
EPSRC, Grant/Award Number: EP/P030564/1

## Abstract

The through-thickness conductivity of carbon fiber reinforced polymer (CFRP) composite was increased by incorporating multiwalled carbon nanotubes in the interlaminar region. Carbon nanotubes (CNTs) were dispersed in a polyethylenimine (PEI) binder, which was then coated onto the carbon fiber fabric. Standard vacuum-assisted resin infusion process was applied to fabricate the composite laminates. This modification technique aims to enhance the electrical conductivity in through-thickness direction for the purpose of nondestructive testing, damage detection, and electromagnetic interference shielding. CNT concentrations ranging from 0 to 0.75 wt% were used and compared to pristine CFRP samples (reference). The through-thickness conductivity of the CFRP exhibited an improvement of up to 781% by adopting this technique. However, the dispersion of CNT in PEI led to a viscosity increase and poor wetting properties which resulted in the formation of voids/defects, poor adhesion (as shown in scanning electron micrographs) and the deterioration of the mechanical properties as manifested by interlaminar shear strength and dynamic mechanical analysis measurements.

**KEYWORDS**

conducting polymers, graphene and fullerenes, mechanical properties, nanotubes, surfaces and interfaces, thermosets

## 1 | INTRODUCTION

Damage within composites is often due to shock events causing delamination between plies and is hard to be observed visually or accurately.[1] Thus, structural health monitoring is used to determine the remaining life of a structure. Self-sensing materials have allowed the possibility to detect and self-monitor the strain and damage in the system nondestructively.[2] Carbon fiber reinforced polymer (CFRP) damage is linked with its electrical resistance, as cracks apparition and development reduce composites' conductivity, allowing real-time monitoring of its condition. By detecting early damage, life extension control can be made as well as

damage mitigation to ensure the reliability and safety of CFRP.

Indeed CFRP have high specific strength, excellent Young's modulus, good corrosion resistance, and anti-fatigue properties, making it an alternative material to the conventional metal in many applications including aerospace, automotive and structural engineering.[3] However, CFRP is an anisotropic material that has a low electrical and thermal conductivity, especially in the through-thickness direction due to the nonconductive matrix resin between the carbon fiber plies. This makes it difficult to detect damage inside the composite. Enhanced electrical conductivity in the through-thickness direction would not only allow dynamic structural health monitoring,[4–7] but would also increase the effectiveness of electromagnetic shielding and provide lightning protection.[8–13]

Researchers have integrated several types of carbon-based nanofillers, such as carbon nanotubes (CNTs), graphene, and carbon black to improve the electrical properties of the CFRP.[14–18] Nanofillers have a very high surface area to volume ratio, leading to the high interfacial area and thus to better interfacial adhesion. However, CNT agglomeration can prevent the formation of an extensive interphase area and introduce defects. This has been an issue for the effective fabrication of conductive polymer composites (CPC), epoxy systems have been reported in the literature.[19,20] Nevertheless, nanosize particles allow for early particle percolation threshold, at very low wt%.[21] CNT, in particular, are also high aspect ratio objects, driving down further the wt% required to reach the percolation threshold,[22] and therefore can be used to provide a fair and stable conductivity in composite structures. Chapartegui et al.[23] analyzed the vitrification time of neat epoxy and epoxy-based CPC CNT by rheometry during isothermal curing at 60°C. The authors reported that at low filler content that is, 0.1 wt%, CNT tended to decrease the gelation time, whereas for CNT contents over the percolation, the reverse effect was observed. Domingues et al.[24] showed that the use of an electric field during CPC epoxy curing enhanced the CNT agglomeration. They also showed that field-induced CPC reached a higher conductivity. De La Vega et al.[25] investigated the curing of epoxy-based CNT by conductivity coupled with Raman spectroscopy measurements. While subjected to increasing temperature isothermal steps, the conductivity increased along with the degree of curing and the Raman peak shift decreased at each isothermal stage. The authors demonstrated that the shrinkage of the epoxy-based CPC, which induces thermo-compressive strain on the CNT, was revealed by the Raman G' band shift.

The re-agglomeration effect of carbonaceous components in epoxy-based CPC was reported by Schulte for carbon black,[26,27] and CNT.[18] They claimed that filler particles were flocculating within the polymer matrix due to Brownian motion using the colloid particle–to–particle potential energy theory.[27] For particles being dispersed in a liquid/viscous media, London and van der Waals attractive forces compete with the repulsive Coulombic force. At long range, particles have few interactions together. At closer range, Coulombic repulsive forces act as a barrier of potential energy preventing agglomeration. Nevertheless, the barrier can be crossed if the thermodynamic properties are favorable. In this case, van der Waals forces take over, allowing the particles to flocculate. Due to Brownian motion, filler agglomerates grow and build up a percolation network following a fractal dimension law.[18,27] Indeed Ma et al. managed to mitigate the effect of CNT re-agglomeration in epoxy-based CPC by using amino-functionalized CNT, highlighting the importance of surface energy in re-agglomeration inhibition.[28]

The elevation of temperature during curing gives more energy to the system and allows van der Waals secondary interactions to aggregate CNT in bundles to take place in the case of epoxy-based CPC CNT. However, two other features have a large influence on CNT re-agglomeration in CPC-based structures. First, the resin viscosity drops before gelation, allowing for a higher CNT re-agglomeration.[29] Second, the cured composite shrinkage also diminishes the CNT interparticle distance and enhances the conductivity of the epoxy-based CPC. Unfortunately, the heterogeneous resin behavior, due to lower wetting capabilities, leads to a reduction of mechanical properties. Indeed CNT re-agglomeration and preferential epoxy cure drastically increases local viscosity,[30,31] leading to increased porosity and further reduction of mechanical properties, especially in the interlaminar region.

Polyethylene imine (PEI) is a well-known co-curing agent of epoxy and has been used to increase interfacial properties of CFRP by functionalizing carbon fibers[32] and was very recently used to improve epoxy-based CPC CNT composites conductivity[33] due to a better dispersion in solution. In this study, the interlaminar regions of CFRP were modified with CNT/PEI coating having different loadings of CNT in this study. The effect of CNT concentrations on the through-thickness conductivity was investigated by measuring the conductivity using a two-point probe method. Static and dynamic mechanical properties were investigated via interlaminar shear strength (ILSS) and dynamic mechanical analysis (DMA). Scanning electron microscopy (SEM) was also performed to assess the adhesion between the different constituents (carbon fibers, PEI/CNT, epoxy) after breakage.

## 2 | EXPERIMENTAL

### 2.1 | Materials and sample preparation

Figure 1 represents the multiple steps taken in this study. First, an aqueous suspension containing 3 wt% of

predispersed multiwalled carbon nanotube (CNT) (Nanocyl© Aquacyl- AQ0302) was sonicated with an epoxy-compatible polyethylenimine (PEI, MICA A-131-X) aqueous binder from Mica Corporation© (Figure 1 (a)). Cross-ply carbon fiber fabrics from Saertex (X-C-218 g/m$^2$-1400mm), with TORAY T700 SC 50C 12 K carbon fibers were selected in this study. PEI is well-known for its epoxy-based composite interlayer properties[34] and can easily crosslink with the diglycidyl ether functional group of epoxide resins, providing strong mechanical adhesion at the interphase. The CNT concentration in resin was set at 5%, 10%, and 15% weight in PEI and represented, respectively, 0.25, 0.50, and 0.75 wt% of the overall weight of the composite. The PEI + CNT binder mass was kept constant at 5 wt% of the overall CFRP weight

The targeted overall composition of the laminates is given in Table 1.

The aqueous binder + CNT solutions were then carefully applied on the carbon fiber fabrics and dried for

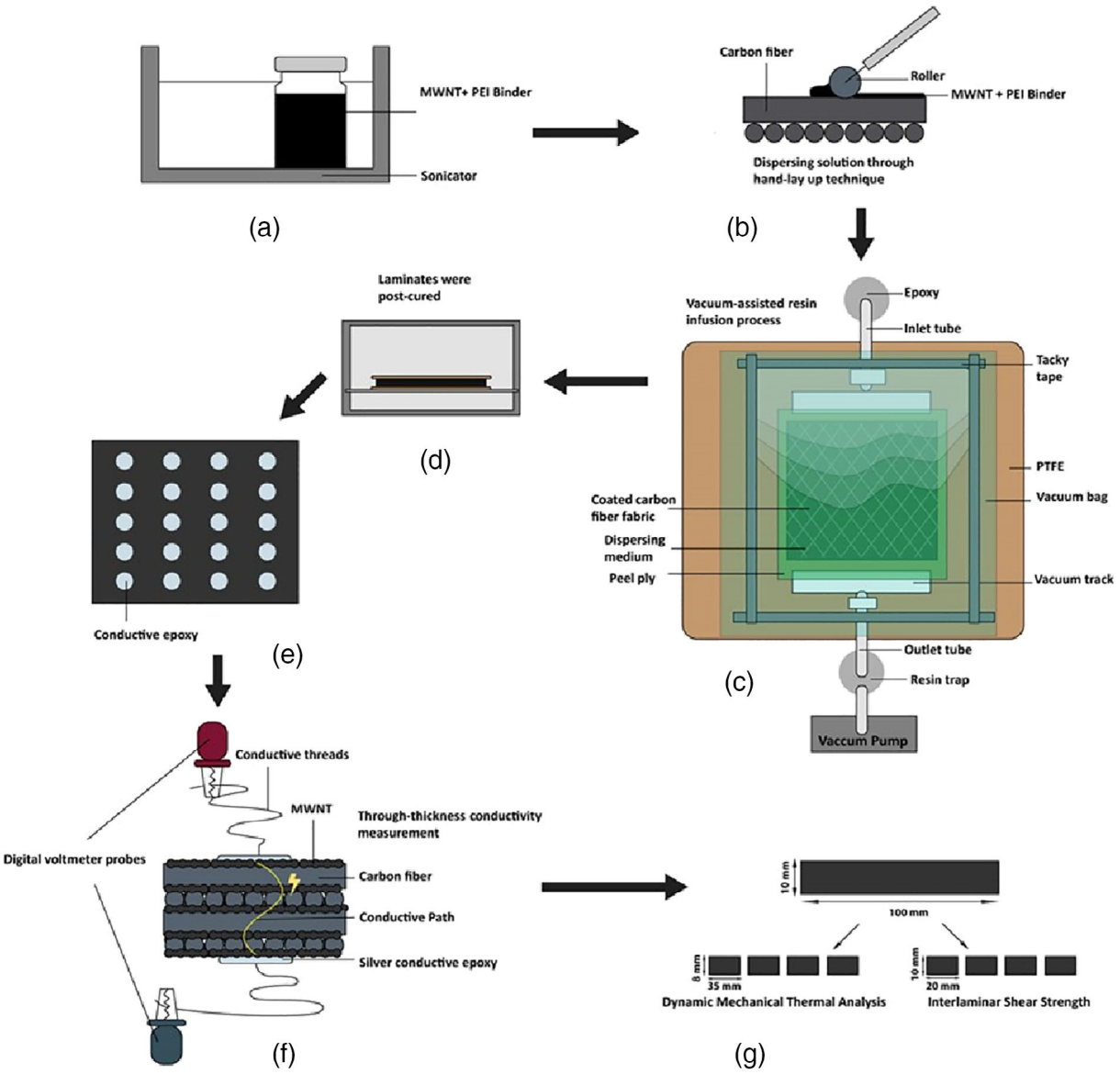


**FIGURE 1** Schematics of overall CFRP preparation and testing: (a) CNT dispersion in PEI binder in a sonication bath. (b) Casting of CNT/PEI solution on carbon fiber fabric. (c) VARI processing after the coated fabric was dried. (d) Cure and post-cure of the composite. (e) Polishing (up to carbon fiber were apparent) and conductive epoxy application on both faces of laminates. (f) Two-point probe through-thickness conductivity measurements. (g) DMA and ILSS testing. (CFRP, carbon fiber reinforced polymer; CNT, carbon nanotube; DMA, dynamic mechanical analysis; ILSS, interlaminar shear strength; PEI, polyethylenimine; VARI, vacuum-assisted resin infusion) [Color figure can be viewed at wileyonlinelibrary.com]

24 h at room temperature under fume hood convection (Figure 1(b)) followed by 2 h heating at 40°C in an oven. The CFRP plates were manufactured by vacuum-assisted resin infusion molding at room temperature using an Easy Composites© infusible epoxy resin (IN2) mixed with a slow hardener (AT30) in 100:30 ratio (Figure 1(c)). The laminates were then cured for 24 h at ambient temperature before post curing for 2 h at 40 and 50°C followed by 4 h at 60°C (Figure 1(d)). In this process, the processing temperatures were kept fairly low to reduce the influence of CNT re-agglomeration.

The top and bottom surfaces of each laminate were polished to remove the excess epoxy resin and expose the conductive path.[35,36] A conductive silver epoxy adhesive and hardener (CircuitWorks© CW2400) were mixed at a 1:1 ratio and painted on the plates at 20 equally distributed points with conductive threads (Kitronik© Electro Fashion 2744) on both sides before leaving to cure overnight (Figure 1(e)). After measuring the through-thickness electrical conductivity (Figure 1(f)), the laminates were cut into small specimens for DMA and ILSS analysis (Figure 1(g)).

## 2.2 | Characterization

Silver conductive epoxy and conductive threads were used with a digital multimeter (MS8217 Autorange) to measure the electrical resistance between the two electrical contacts in the through-thickness direction. The two-point probe method is commonly used for CFRP electrical measurement, as the contact resistance is low with respect to the overall resistance.[36–40] A grid of 20 through-thickness electrical resistance data was assessed on each plate, taking into consideration the resistivity of the conductive threads. The plate thickness was measured at each point for resistivity calculation by a digital micrometer. The interfacial mechanical properties of the CFRP specimens were investigated through ILSS tests performed according to ISO 14130. The tests were carried out using Instron 3369 at a crosshead speed of 1 mm/min. DMA was performed according to ASTM D4065-12 to investigate the viscoelastic properties. The test was carried out on samples (dimension: $35 \times 8 \times 2$ mm$^3$) using DMA 8000 (Perkin Elmer©), in three-point bending mode at 1 Hz and 20 μm displacement. A temperature sweep from 25 to 150°C at a rate of 5°C/min was performed. Glass transition temperature (*Tg*) and tan delta were determined and plotted in the Pyris software to obtain the damping properties of the CFRP.

SEM was acquired as a means of qualitatively assessing failure morphologies following by Interlaminar shear stress testing. The tested/fracture surfaces of the CFRP composite samples were visualized by a Zeiss Crossbeam 550 focused ion beam SEM at an electron excitation voltage of 5 kV. Prior to the examination, the fracture surfaces were sputter-coated with a thin evaporated layer of gold, reaching a thickness of approximately 100 Å using an AGAR automatic Sputter Coater B7341.

# 3 | RESULTS AND DISCUSSION

## 3.1 | Through-thickness electrical conductivity

The through-thickness electrical conductivity of the carbon fiber/epoxy plates loaded with CNTs was measured and compared to the pristine CFRP as reference. The average through-thickness conductivity of the carbon fiber/epoxy plates loaded with CNT shows a sevenfold increase compared with the pristine sample (Figure 2). The conductivity continues to increase from 0.032 S/m for the pristine CFRP sample, up to 0.216 S/m at CNT loading of 0.25 wt% and to increase to 0.25 S/m at 0.5 wt % loading. However, the conductivity surprisingly decreases when the CNT loading is further increased to 0.75 wt% (0.226 S/m). The authors postulate this is due to an increase in viscosity, leading to more porosity and therefore a looser conductive network. The conductivity of the CFRP increases logarithmically as the CNT loading increases up to 0.5 wt%. This behavior agrees with the

**TABLE 1** Weight composition of CFRP plates

| Laminate name | Fiber wt% | CNT wt% | Binder wt% | Resin wt% |
|---|---|---|---|---|
| Pristine CFRP | 58.00 | — | — | 42.00 |
| PEI binder only | 58.00 | — | 5.0 | 37.00 |
| 0.25 wt% CNT loading + PEI binder | 58.00 | 0.25 | 4.75 | 37.00 |
| 0.50 wt% CNT loading + PEI binder | 58.00 | 0.50 | 4.50 | 37.00 |
| 0.75 wt% CNT loading + PEI binder | 58.00 | 0.75 | 4.25 | 37.00 |

Abbreviations: CFRP, carbon fiber reinforced polymer; CNT, carbon nanotube; PEI, polyethylenimine.

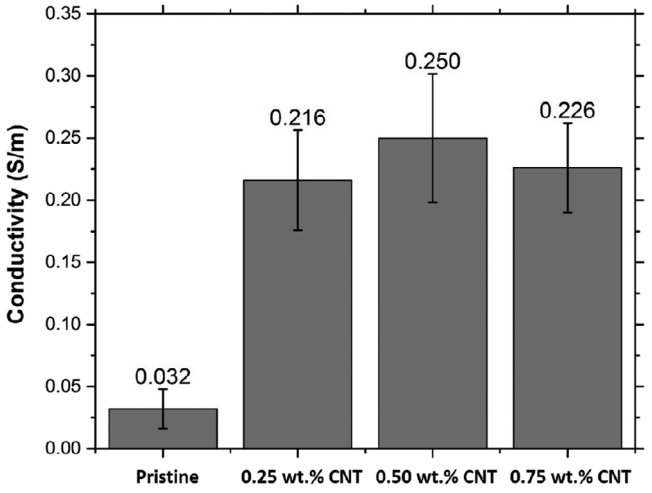


**FIGURE 2** Through-thickness electrical conductivity of pristine and PEI/CNT loaded CFRP. (CFRP, carbon fiber reinforced polymer; CNT, carbon nanotube; PEI, polyethylenimine)

study from Allaoui and Zeng.[14,41] The interfacial conductive coating improves the through-thickness electrical conductivity by establishing a localized conductive network within the CFRP. The electron transfer is greatly improved at the closest conductive areas between the carbon fibers' layers. In a CNT network, the main conduction mode is tunneling conductivity,[42–44] that explains the logarithmic relationship between conductivity and CNT loading, as the latter directly influences the minimal interparticle distance between the CNT.[45]

Allaoui and Zeng[14,41] studies reported that the CNT percolation threshold ranged from 0.5 to 2.5 wt%. In fact, the uniformity and dispersion of the CNT can significantly influence the percolation threshold. The more uniform the dispersion, the lower the percolation threshold.[46,47] Ma et al. reported a large scatter regarding CNT percolation threshold value for epoxy-based CPC.[48] Therefore, in this study, several CNT loadings were chosen above the minimum percolation threshold to ensure a better through-thickness conductivity. However, this also meant that at such high CNT loadings agglomeration would occur. This can particularly be seen in the case of the 0.75 wt% CNT laminate, which displays lower conductivity than the 0.50 wt% CNT one. It should also be noted that the standard deviation of the three CNT-loaded sets is high and put in doubt the significance of this trend, as often observed when working with CNT due to re-agglomeration issues.

Poor dispersion of CNT can lower the effectiveness of the enhancement of electrical properties in the composites because it could increase agglomeration. Gojny et al.[49] had experienced that high percentage-loading of nanofiller, such as carbon black and CNT, could deteriorate the electrical and mechanical properties due to the agglomeration of the nanofiller. In agreement with this, a decrease in conductivity was observed as the CNT loading reached 0.75 wt%. The higher loading of CNT increased the viscosity of the resin, leading to the formation of CNT aggregates, which adversely affected the wetting of the carbon fibers forming voids at the interface.[33–36] The coefficient of variation of the CNT coated samples were almost four times lower than the pristine sample, due to a more homogeneous conductive network, as much as a lower minimal interlayer distance, responsible for the higher conductivity of the CNT-based samples.

## 3.2 | Interlaminar shear properties

Figure 3(a) displays displacement–load curves, while Figure 3(b) represents the average ILSS for each type of sample. The incorporation of the PEI coating (with and without CNT) reduced the maximum load and shear stress that the specimens can withstand before failing. The average ILSS of the CNT-coated samples was six to eight times smaller than the pristine sample.

On one hand, PEI can easily bind to epoxide groups and is often used as a co-curing and hardening agent for epoxy.[50] On the other hand, recent studies highlighted excellent chemical compatibility between CNT and PEI[51,52] allowing for high dispersion of CNT into PEI under sonication. These advantages drove the authors to use PEI as a binder to epoxy-based CPC CNT nanocomposite.

However, Figure 3(b) undoubtedly describes a severe reduction of ILSS. Pristine samples had an ILSS over five times higher than the epoxy-based CNT CFRP samples, including PEI. This adverse role played by the PEI could be explained by its segregation at the interphase, drastically reducing the wetting ability of epoxy to the PEI/CNT phase. Further addition of CNT in the PEI increased the viscosity of the PEI/CNT phase, further lowering the ILSS.

These results are hardly surprising as in the literature, many through-thickness conductivity studies reported significant reduction of mechanical properties[36,53–61] (or did not report on mechanical properties[3,62–66]).

Indeed, adding conductive nanoparticles in polymeric matrices can severely increase the viscosity of the polymeric matrix, leading to a higher porosity and weak fiber/matrix interfacial adhesion (as shown in the following SEM investigation). This results in a significant drop in mechanical properties, as has been shown in ILSS measurements (Figure 3) and is further demonstrated in the following DMA investigation.

## 3.3 | Viscoelastic properties

Five samples per set were tested in three-point bending mode using a DMA in temperature sweep mode (5°C/min).

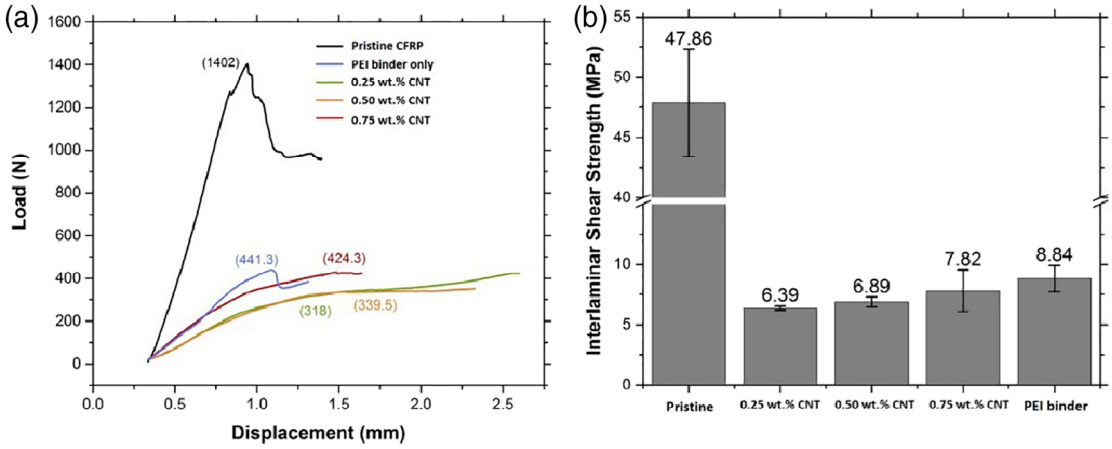


**FIGURE 3** (a) Displacement/load curves (b) Summary of interlaminar shear strength (ILSS) properties for pristine CFRP compared to CNT/PEI and PEI only CFRP samples. (CFRP, carbon fiber reinforced polymer; CNT, carbon nanotube; PEI, polyethylenimine) [Color figure can be viewed at wileyonlinelibrary.com]

The Tan delta results are presented in Figure 4 for all cases. The Tan delta measures the damping factor, which is the ratio of the viscous response to the elastic response of the material. Three critical indicators can be noticed in Figure 4: the peak intensity, the glass temperature, and the Tan delta peak width. In all examined cases, the same trend was noticed: first the pristine CFRP samples have the highest values, followed by PEI binder only samples, then by 0.75, 0.5, and finally 0.25 wt% CNT samples. This trend is the same as for the ILSS results.

Tan delta is associated with the internal energy dissipation of the matrix and filler interphase.[67] The width of the tan $\delta$ peaks increased significantly in the CNT loaded composites, which indicates enhanced heterogeneity. A high but narrow peak describes a homogeneous CFRP interface with a good adhesion between the fiber and the matrix, which is the case of the pristine samples. Also, the *Tg* drift at lower temperature in case of the CNT loaded samples is an indicator of a lower reversible energy storage capacity (Gibbs free energy).

The introduction of PEI in the composite had several effects at the interphase: PEI is more flexible than epoxy and was segregated in the interlaminar region. The tan $\delta$ peak decreased significantly in comparison to pristine samples, which can be attributed to the participation of PEI in the curing mechanism of the epoxy resin, bringing nonhomogeneity to the crosslinked network.[68] The three-phase system that is, carbon fibers, PEI, and epoxy, led to a more heterogeneous material, increasing the local stiffness difference at the interphase. Finally, the carbon fiber sizing was not tailored for PEI adhesion, further reducing the interfacial adhesion and the energy transfer ability of the composite.

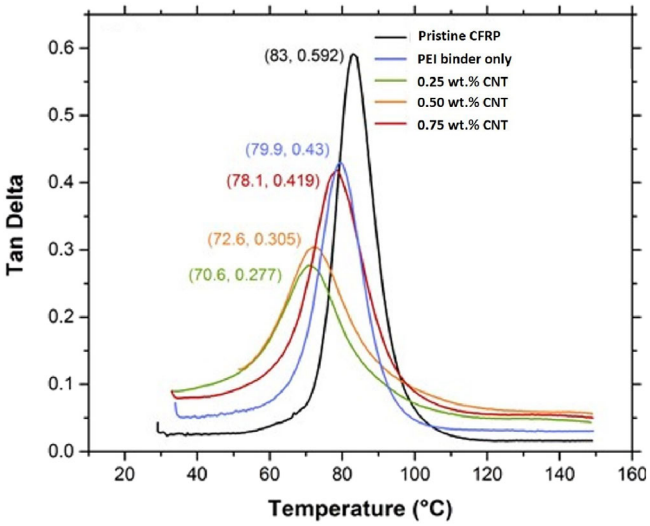


**FIGURE 4** DMTA results of pristine and PEI/epoxy-based CNT CFRP samples: Tan delta versus temperature curves. (CFRP, carbon fiber reinforced polymer; CNT, carbon nanotube; PEI, polyethylenimine) [Color figure can be viewed at wileyonlinelibrary.com]

The addition of CNT in the PEI binder had two distinct effects: first, it drastically increased the PEI binder viscosity, and second, it stiffened the material. These antagonistic effects are responsible for the trend regarding CNT loading. We hypothesized that adding a small amount of CNT will cause a significant viscosity increase,[69] reducing wetting and interphase adhesion, while adding more would help stiffen the CNT/PEI phase as the CNT can occupy free volumes[70] and limit polymeric chain mobility, leading to better stress transfer.

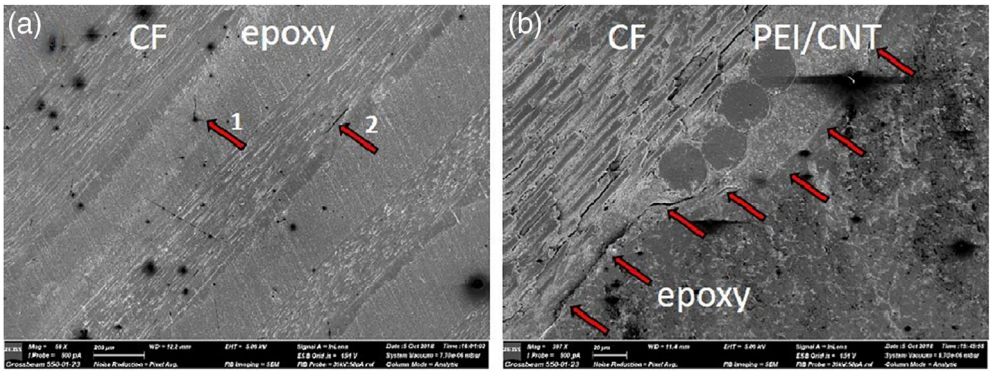


**FIGURE 5** SEM cross-section of (a) Pristine and (b) 0.5 wt% CNT/PEI CFRP samples after the ILSS test. The red arrows represent different fracture mechanisms. (CFRP, carbon fiber reinforced polymer; CNT, carbon nanotube; ILSS, interlaminar shear strength; PEI, polyethylenimine; SEM, scanning electron microscopy) [Color figure can be viewed at wileyonlinelibrary.com]

### 3.4 | SEM observation

The fracture surfaces of the tested/failed ILSS specimens were analyzed using SEM in order to investigate the fracture morphology and the failure mechanisms. Note that all imaged fracture surfaces were taken from similar areas of the failed ILSS specimens, about 2 mm away from the samples' center, for means of comparison.

As the SEM images indicate, there is a clear fractographic difference between the fracture surfaces of a pristine CFRP composite, which exhibits a typical brittle behavior (Figure 5(a)), and the fracture surface of the CNT loaded CFRP.

In Figure 5(a), two different crack initiation mechanisms are reported. In Case 1, a void (black dot) in the matrix acted as initiator. The presence of voids in the epoxy matrix is inherent to the vacuum-assisted resin infusion (VARI) processing used in this study. In Case 2, crack development occurs within the fiber-rich region. It is probable that the composite, which was only under vacuum during the process, was not fully impregnated and nonwetted carbon fibers allowed for crack apparition within the composite.

Figure 5(b) represents a CFRP with 0.5 wt% CNT segregated within the PEI binder, which was located at the carbon fiber interphase. The red arrows highlight a macro crack running throughout the picture. We can see that the crack is not occurring at the carbon fiber/PEI interface but between the PEI and the epoxy, due to a shear ductile failure mechanism. As the PEI/CNT phase was highly viscous, epoxy was not able to diffuse therein. It should be noted that PEI, which is a co-curing agent of epoxy resin, should have led to a higher local crosslinking density at the interphase, and could have been beneficial to the interfacial mechanical properties. However, in the present case the influence of CNT on the viscosity has been predominant. The lack of cohesion between the PEI and epoxy phases is responsible for the low mechanical properties noticed previously.

## 4 | CONCLUSIONS

In this study, the through-thickness electrical conductivity of CFRP was improved by an interlaminar modification route. CNT particles were coated on dry CF reinforcement fabrics with the aid of a PEI binder. PEI also acted as a co-curing agent for epoxy along with the amine hardeners. The PEI/CNT layer in the interlaminar region helped to transfer electricity through the resin-rich interlayers in the through-thickness direction. The scope of a process that could be easily scaled up industrially led us to select VARI processing which is often used to manufacture large structures. The through-thickness electrical conductivity was increased by close to 800% for 0.5 wt % CNT samples compared to the pristine CFRP. The observed decrease in through-thickness conductivity for the 0.75 wt% CNT samples showed the limits of the CNT dispersion in PEI.

However, the mechanical properties of the PEI/CNT CFRP were significantly reduced, and the presence of PEI in the interlaminar region reduced the ILSS over five times. The benefits though from a higher curing density at the PEI/CNT-epoxy interphase were largely overshadowed by the tremendous increase in viscosity, leading to CNT agglomeration, poor wetting and void formation.

The addition of CNT further reduced the ILSS due to viscosity rise and poor wetting, but the addition of more CNT allowed for a stiffened interphase, which slightly increased the ILSS at higher CNT loadings. This trend was confirmed in DMA, as it highlighted the heterogeneous aspect of CNT loaded CFRP samples. Finally, SEM observations unequivocally showed the lack of adequate adhesion between the PEI binder and epoxy.

In future work, the issue of segregated phases (PEI/CNT and epoxy) should be addressed for example, mixing PEI and some epoxy in a solvent prior to adding and dispersing CNT. The processing method could also be reviewed, and a better consolidation could be obtained with high pressure processing.

## ACKNOWLEDGMENTS

The authors acknowledge the use of the Cryo FIB/SEM bought with the EPSRC grant EP/P030564/1 and Dr. Thomas Glen for help with image acquisition.

## ORCID

*Colin Robert* https://orcid.org/0000-0001-5035-6134
*Dipa Ray* https://orcid.org/0000-0002-2353-9581
*Norbert Radacsi* https://orcid.org/0000-0002-7358-951X
*Vasileios Koutsos* https://orcid.org/0000-0002-2203-8179

## REFERENCES

[1] M. Tehrani, A. Boroujeni, T. Hartman, T. Haugh, S. Case, M. Al-Haik, *Compos. Sci. Technol.* **2013**, *75*, 42.
[2] H. Zhang, E. Bilotti, P. T, *Nanocomposites* **2015**, *1*, 167.
[3] X. Cheng, T. Yokozeki, L. Wu, H. Wang, J. Zhang, J. Koyanagi, Z. Weng, Q. Sun, *Compos. Part A: Appl. Sci. Manuf.* **2016**, *90*, 243.
[4] S. Wang, D. Chung, *Compos. Interfaces* **2002**, *9*, 51.
[5] L. Ci, J. Bai, *Compos. Sci. Technol.* **2006**, *66*, 599.
[6] J. Wen, Z. Xia, F. Choy, *Composites, Part B* **2011**, *42*, 77.
[7] S. Han, D. Chung, *Compos. Sci. Technol.* **2011**, *71*, 1944.
[8] P. Jana, A. Mallick, S. De, *Composites* **1991**, *22*, 451.
[9] X. Luo, D. Chung, *Composites, Part B* **1999**, *31*, 227.
[10] N. C. Das, T. Chaki, D. Khastgir, A. Chakraborty, *Adv. Poly. Technol.* **2001**, *20*, 226.
[11] A. Katunin, K. Krukiewicz, R. Turczyn, P. Sul, M. Bilewicz, *IOP Conf. Ser.: Mater. Sci. Eng.* **2017**, *201*, 012008.
[12] C. Metzner and C. Karch, presented at Int. Conf. on Lightning Protection, Shanghai, **2014**.
[13] T. R. Pozegic, J. V. Anguita, I. Hamerton, K. D. I. Jayawardena, J.-S. Chen, V. Stolojan, P. Ballocchi, R. Walsh, S. R. P. Silva, *Sci. Rep.* **2016**, *6*, 37334.
[14] A. Allaoui, S. Bai, H. Cheng, J. Bai, *Compos. Sci. Technol.* **2002**, *62*, 1993.
[15] H. Yang, J. Gong, J. X. Xin Wen, Q. Chen, Z. Jiang, N. Tian, T. Tang, *Compos. Sci. Technol.* **2015**, *113*, 31.
[16] K. Hamdi, Z. Aboura, W. Harizi, K. Khellil, *J. Compos. Mater.* **2018**, *52*, 1495.
[17] X. Cheng, V. Kumar, T. Yokozeki, T. Goto, T. Takahashi, J. Koyanagi, L. Wu, R. Wang, *Compos. Part A: Appl. Sci. Manuf.* **2016**, *82*, 100.
[18] J. Sandler, M. Shaffer, T. Prasse, W. Bauhofer, K. Schulte, A. Windle, *Polymer* **1999**, *40*, 5967.
[19] P. Pötschke, F. Mothes, B. Krause, B. Voit, *Polymer* **2019**, *11*, 189.
[20] N. Siddiqui, C. Li, Y. Yu, P. Ma and J. Kim, presented at ICCM Int. Conf. on Composite Materials, Edinburgh, **2009**.
[21] X. Jing, W. Zha, L. L, *J. Mater. Sci. Lett.* **2000**, *19*, 377.
[22] Y. Mamunya, N. Lebovka, M. Llsunova, E. Lebedev, A. Rybak, G. Boiteux, *J. Nanostructured Polym. Nanocomposites* **2008**, *4*, 21.
[23] M. Chapartegui, S. Florez, C. Elizetxea, M. Fernandez, A. Santamaria, *Soc. Plast. Eng.* **2011**.
[24] D. Domingues, E. Logakis, A. Skordos, *Carbon* **2012**, *50*, 2493.
[25] A. De La Vega, J. Kovacs, W. Bauhofer, K. Schulte, *Compos. Sci. Technol.* **2009**, *69*, 1540.
[26] R. Schueler, J. Petermann, K. Schulte, H.-P. Wentzel, *Macromol. Symp.* **1996**, *104*, 261.
[27] R. Schueler, J. Petermann, K. Schulte, H.-P. Wentzel, *J. Appl. Polym. Sci.* **1997**, *63*, 1741.
[28] P.-C. Ma, S.-Y. Mo, B.-Z. Tang, J.-K. Kim, *Carbon* **2010**, *48*, 1824.
[29] M. Morais, A. Oliva-Avilés, M. Matos, V. Tagarielli, S. Pinho, C. Hübner, F. Henning, *Carbon* **2019**, *150*, 153.
[30] J. Kim, D. Seong, T. Kang, J. Youn, *Carbon* **2006**, *44*, 1898.
[31] L. Cividanes, E. Simonetti, M. Moraes, F. Fernandes, G. Thim, *Polym. Eng. Sci.* **2013**, *54*, 2461.
[32] L. Ma, L. Meng, G. Wu, Y. Wang, M. Zhao, C. Zhang, Y. Huang, *Compos. Sci. Technol.* **2015**, *114*, 64.
[33] Y. Chen, W. Wei, Y. Zhu, J. Luo, L. Liu, *Compos. Sci. Technol.* **2019**, *170*, 25.
[34] L. Yan, X. Gao, F. Wahid-Pedro, J. T. E. Quinn, Y. Meng, Y. Li, *J. Mater. Chem. A* **2018**, *6*, 14315.
[35] M. Louis, S. Joshi, W. Brockmann, *Compos. Sci. Technol.* **2001**, *61*, 911.
[36] K. Everson, K. A. Akbar, Y. Sanghyun, R. Wang, J. Ma, P. Olivier, G. Nathalie, C. H. Wang, *Compos. Part A: Appl. Sci. Manuf.* **2015**, *69*, 72.
[37] R. Moriche, S. G. Prolongo, M. Sanchez, A. Jimenez-Suarez, M. Campo, A. Urena, *J. Vis. Exp.* **2016**, *117*, 1.
[38] P. Cong, P. Xu, S. Chen, *Constr. Build. Mater.* **2014**, *52*, 306.
[39] W. Qin, F. Vautard, L. T. Drzal, J. Yu, *Composites, Part B* **2015**, *69*, 335.
[40] Y. Hirano, T. Yamane, A. Todoroki, *Compos. Sci. Technol.* **2016**, *122*, 67.
[41] X. Zeng, X. Xu, P. M. Shenai, E. Kovalev, C. Baudot, N. Mathews, Y. Zhao, *J. Phys. Chem.* **2011**, *115*, 21685.
[42] X. W. Zhang, Y. Pan, Q. Zheng, X. Yi, *J. Polym. Sci. Part B* **2000**, *38*, 2739.
[43] M. Knite, V. Teteris, A. Kiploka, J. Kaupuzs, *Sens. Actuators A* **2004**, *110*, 142.
[44] M. Knite, V. Tupureina, A. Fuith, J. Zavickis, V. Teteris, *Mater. Sci. Eng. C* **2007**, *27*, 1125.
[45] C. Robert, I. Pillin, M. Castro, J.-F. Feller, *J. Compos. Sci.* **2019**, *3*, 109.
[46] J. Li, P. Ma, W. Chow, C. To, B. Tang, J. Kim, *Adv. Funct. Mater.* **2007**, *17*, 3207.
[47] M. Bryning, M. Islam, J. Kikkawa, A. Yodh, *Adv. Mater.* **2005**, *17*, 1186.
[48] P. C. Ma, N. A. Siddiqui, G. Marom, J.-K. Kim, *Compos. Part A: Appl. Sci. Manuf.* **2010**, *41*, 1345.
[49] F. H. Gojny, M. H. Wichmann, B. Fiedler, K. Schulte, *Compos. Sci. Technol.* **2005**, *65*, 2300.
[50] W. Choi, K. Min, C. Kim, Y. Ko, J. Jeon, H. Seo, Y. Park, M. Choi, *Nat. Commun.* **2016**, *7*, 12640.
[51] S. Duan, R. Yue, Y. Huang, *Talanta* **2016**, *160*, 607.
[52] A. Zestos, C. Jacobs, E. Trikantzopoulos, A. Ross, B. Venton, *Anal. Chem.* **2014**, *86*, 8568.
[53] Y. Hirano, T. Yokozeki, Y. Ishida, T. Goto, T. Takahashi, D. Qian, S. Ito, T. Ogasawara, M. Ishibashi, *Compos. Sci. Technol.* **2016**, *127*, 1.
[54] I. Gaztelumendi, M. Chapartegui, R. Seddon, S. Florez, F. Pons, J. Cinquin, *Composites, Part B* **2017**, *122*, 31.
[55] V. Kumar, T. Yokozeki, T. T. T. Goto, S. R. Dhakate, S. B. P, *Compos. Sci. Technol.* **2017**, *152*, 20.

[56] P. Latko-Durałek, K. Dydek, P. Bolimowski, E. Golonko, P. Durałek, R. Kozera, B. A, *Mater. Sci. Eng.* **2018**, *406*.
[57] Z. Zhao, G. Xian, J. Yu, J. Wang, J. Tong, J. Wei, C. Wang, P. Moreira, X. Yi, *Compos. Sci. Technol.* **2018**, *167*, 555.
[58] W. Li, D. Xiang, L. Wang, E. Harkin-Jones, C. Zhao, B. Wang, Y. Li, *RSC Adv.* **2018**, *8*, 26910.
[59] K. Dydek, A. Boczkowska, P. W. M. P. K. K. R. Latko-Durałek, *J. Compos. Mater.* **2020**, *0*, 0.
[60] V. Kumar, S. Sharma, A. Pathak, B. Singh, S. Dhakate, T. Yokozeki, T. Okada, O. T, *Compos. Struct.* **2019**, *210*, 581.
[61] M. Guo, Y. X, *Aerospace* **2018**, *5*, 77.
[62] X. Cheng, T. Yokozeki, L. Wu, J. Koyanagi, H. Wang, Q. Sun, *Compos. Part A: Appl. Sci. Manuf.* **2018**, *105*, 281.
[63] I. Sawi, P. Olivier, P. Demont, B. H, *Compos. Sci. Technol.* **2012**, *73*, 19.
[64] Y. Lin, M. Gigliotti, M. Lafarie-Frenot, J. Bai, D. Marchand, D. Mellier, *Composites, Part B* **2015**, *76*, 31.
[65] F. Pegorin, K. Pingkarawat, M. A, *Compos. Sci. Technol.* **2017**, *150*, 167.
[66] J. Rehbein, P. Wierach, T. Gries, W. M, *Compos. Part A: Appl. Sci. Manuf.* **2017**, *100*, 352.
[67] N. Saba, A. Safwan, M. Sanyang, F. Mohammad, M. Jawaid, O. Alothman, M. Sain, *Int. J. Biol. Macromol.* **2017**, *102*, 822.
[68] X.-C. Zhang, F. Scarpa, R. McHale, H.-X. Peng, *Polymer* **2016**, *87*, 236.
[69] T. Chatterjee, R. Krishnamoorti, *Soft Matter* **2013**, *9*, 9515.
[70] A. Montazeri, N. Montazeri, *Mater. Des.* **2011**, *32*, 2301.

**How to cite this article:** Robert C, Thitasiri WB, Mamalis D, et al. Improving through-thickness conductivity of carbon fiber reinforced polymer using carbon nanotube/polyethylenimine at the interlaminar region. *J Appl Polym Sci*. 2020;e49749. https://doi.org/10.1002/app.49749